Available online at www.sciencedirect.com
ScienceDirect
Journal of Power Sources 174 (2007) 1091–1094
JOURNAL OF POWER SOURCES
www.elsevier.com/locate/jpowsour

Short communication

Sn-based intermetallic materials Performances and mechanisms

S. Naille *, C.M. Ionica-Bousquet, F. Robert, F. Morato, P.-E. Lippens, J. Olivier-Fourcade

Laboratoire des Agrégats Moléculaires et Matériaux Inorganiques (CNRS UMR 5072), Université Montpellier II, CC 015, Place E. Bataillon, 34095 Montpellier Cedex 5, France

Available online 22 June 2007

Abstract

Ni_3Sn_4 and $CoSn_2$ which are two Sn-based intermetallic compounds with different crystal structures have been tested as future negative electrodes for lithium-ion batteries. Various two-step reactions occur during the first discharge of these two electrodes. The first discharge shows good specific capacities: 515 mAh g^{-1} for the Ni_3Sn_4 electrode and 606 mAh g^{-1} for the $CoSn_2$ electrode. These reactions lead to the formation of Li_7Sn_2, a Li-rich Li_xSn alloy characterized by ^{119}Sn Mössbauer spectroscopy.

Keywords: Sn-based intermetallic compounds; Lithium-ion batteries; ^{119}Sn Mössbauer spectroscopy

1. Introduction

As a negative electrode for Li secondary batteries, Sn processes a maximum Li uptake of $Li_{4.4}Sn$ corresponding to a theoretical specific capacity of 993 mAh g^{-1}, much higher than that of graphite (372 mAh g^{-1}). The Sn anode application has nevertheless been hindered by rapid capacity decay upon the charge and discharge cycles. The major problem is the severe volume change during the alloying (Li_xSn) and dealloying reactions. Research for improved electrode materials has led to Sn-based amorphous oxides: SnO, SnO_2, $SnB_xP_yO_z$ [1–3], Sn–M–C (M = Fe, Mn) composites [4,5] and Sn_xM_y alloys (M = Ni, Cu) [6,7]. These materials operate on the basis of alloying reactions described as displacement reactions in which Sn forms a lithium alloy (Li_xSn) and in which a nanosize matrix is created. This matrix may buffer the volume expansion of the Li_xSn active phase. Another interesting feature of these negative electrode materials is the electrochemically driven solid-state amorphisation that takes place during the first alloying period. The interest in Sn-based anodes has increased since Sony recently developed a new hybrid lithium-ion battery, named Nexelion™ [8]. This new battery uses a Sn-based amorphous anode consisting of multiple elements such as tin, cobalt, carbon, where the elements are mixed at a nanometer level, inducing a 30% increase in capacity per volume ratio compared to conventional lithium-ion batteries.

In this work, two transition metal–tin-based intermetallics, i.e. Ni_3Sn_4 and $CoSn_2$ were tested as future negative electrode materials to use the large reversible lithium storage capacity of tin as well as the inactive matrix effect of transition metals to improve cycling performances. Furthermore, these two compounds have different crystal structures. Indeed, Ni_3Sn_4 crystallizes in the monoclinic system, space group *C*2/*m*, whereas $CoSn_2$ crystallizes in the tetragonal system, space group *I*4/*mcm*.

2. Experimental

Elemental Ni (Merck, 99.5%), Co (Merck, 99%) and Sn (Aldrich, 99%) powders were mixed in the Ni_3Sn_4 and $CoSn_2$ compositions. The powder mixtures were then mechanically milled for 10 min in a Pulverisette-7 planetary micro-mill with agate balls and vials under argon atmosphere. Finally, the mechanically alloyed powders were fired in a tube-type furnace under controlled atmosphere. Temperature programs were 4 h at 500 °C for Ni_3Sn_4 and 5 h at 500 °C for $CoSn_2$.

Samples were characterized by X-ray powder diffraction, for phase identification and purity, with a Phillips θ–2θ diffractome-

* Corresponding author.
E-mail address: sebastien.naille@univ-montp2.fr (S. Naille).

0378-7753/$ – see front matter © 2007 Elsevier B.V. All rights reserved.
doi:10.1016/j.jpowsour.2007.06.040

ter using Cu Kα radiation (λ = 1.5418 Å) and nickel filter. We have also determined the size of the X-ray coherent domains from the width of the powder diffraction peaks using the fundamental parameters approach proposed by Cheary and Coelho [9]. This procedure is based on the Scherrer method using the full width at half-maximum of the broadened peaks and taking into account experimental broadening due to instruments.

Electrochemical lithium insertion/extraction tests were carried out with (Li/$LiPF_6$ 1 M (EC:PC:3DMC)/material) Swagelock^{TM}-type cells assembled inside an argon-filled glove box. Cathodes were prepared as 7 mm diameter pellets by pressing a mixture made up of 80 wt.% pristine materials, 10 wt.% PTFE binder, and 10 wt.% carbon black to improve the mechanical and electronic conduction properties. Electrochemical discharge/charge curves were recorded on a multichannel Mac Pile II system under galvanostatic conditions at a rate of 1 Li/20 h (*C*/20).

Pristine materials and electrodes at the end of the first discharge were characterized by ^{119}Sn Mössbauer spectroscopy at room temperature in transmission mode with a classical EG&G constant acceleration spectrometer. The γ-ray source was $Ca^{119m}SnO_3$. The velocity scale was calibrated using the magnetic sextet spectrum of a high-purity iron foil absorber and ^{57}Co(Rh) as the source. The isomer shifts are given relative to $BaSnO_3$ which is used as the standard reference. As for the electrochemically inserted samples, the measurements were performed *ex situ* in a specific sample holder. All spectra were fitted to Lorentzian profiles by the least-squares method [10] and the quality of the fit was controlled by the usual χ^2 test.

3. Results and discussion

The X-ray diffraction patterns of the synthesized alloys are given in Fig. 1. Every diffraction peak was indexed for the Ni_3Sn_4 phase (JCPDS no. 04-0845) with $a = 12.187(13)$ Å, $b = 4.055(5)$ Å, $c = 5.216(7)$ Å and $\beta = 105.19(5)^\circ$ and also for the $CoSn_2$ phase (JCPDS no. 25-0256) with $a = 6.364(2)$ Å and $c = 5.456(1)$ Å.

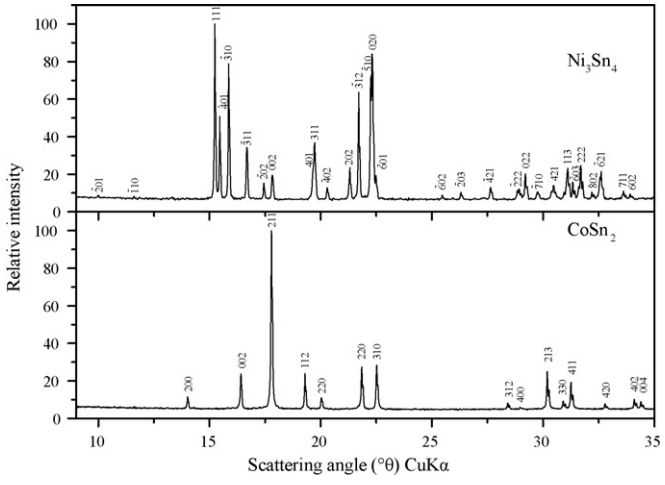

Fig. 1. X-ray diffraction patterns of Ni_3Sn_4 and $CoSn_2$. The sizes of their coherent domains have been estimated to be about 1444 and 1222 Å, respectively, using the Scherrer method from the width of diffraction peaks.

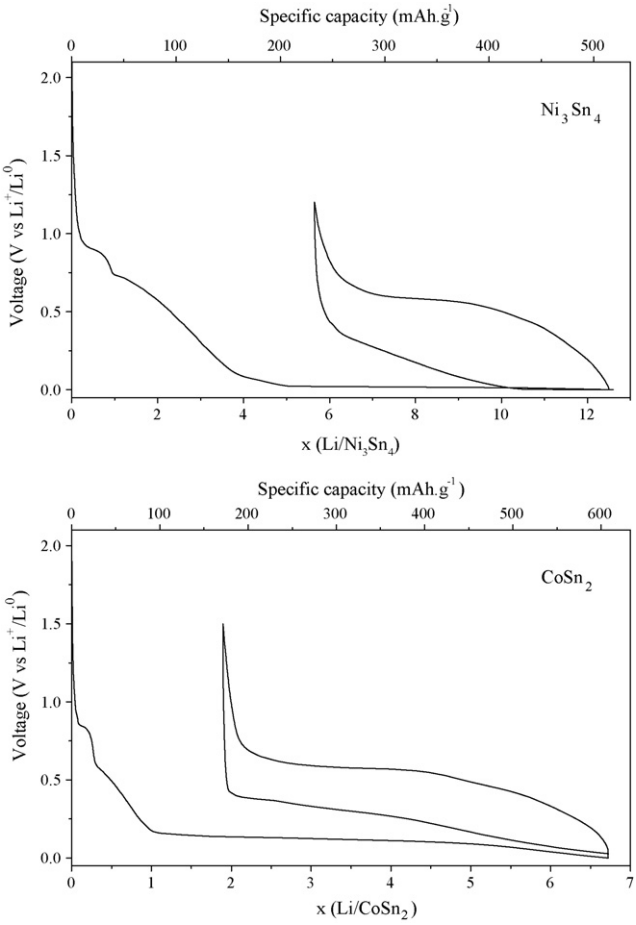

Fig. 2. Discharge–charge curves of Ni_3Sn_4 and $CoSn_2$ electrode materials.

The charge–discharge curves of the Ni_3Sn_4 and $CoSn_2$ samples are given in Fig. 2. The first discharge capacity is 515 mAh g^{-1} and the reversible capacity of the first charge cycle is 282 mAh g^{-1} for the Ni_3Sn_4 electrode. In the case of the $CoSn_2$ electrode, these capacities are 606 and 434 mAh g^{-1}, respectively. Fig. 3 illustrates the cycling behavior of the two electrodes. It can be seen that the specific capacity of Ni_3Sn_4 electrode drops rapidly and continuously without stabilizing.

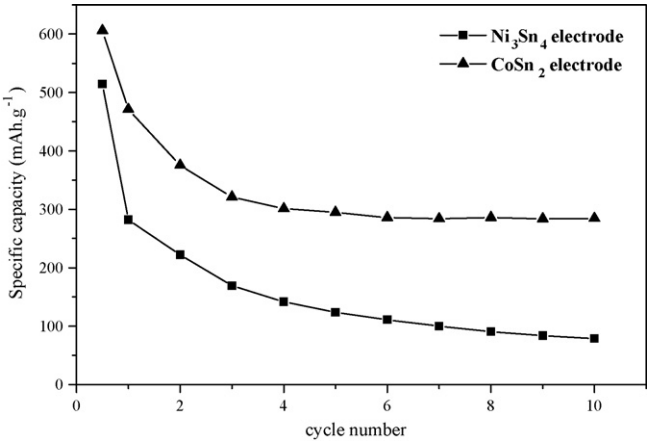

Fig. 3. Cycle performances of Ni_3Sn_4 and $CoSn_2$ electrodes.

As a contrary, the $CoSn_2$ electrode stabilizes after a few cycles to a specific capacity of 285 mAh g^{-1}.

The discharge potential of the electrodes falls quickly to around 0.8 V versus Li. It is due to an electrolyte decomposition reaction that occurs on the surface of carbon, which leads to the formation of a passivating layer, referred to as a solid electrolyte interface [11]. The first discharge of the Ni_3Sn_4 electrode proceeds with a two-step reaction. The first reaction is probably due to a solid-solution insertion reaction which would lead to the formation of a $Li_xNi_3Sn_4$ phase, in which the local environment of the tin atoms are not changed as shown by ^{119}Sn Mössbauer spectroscopy [12]. This reaction would take place up to 4 Li inserted. This is followed by a plateau right above 0.0 V corresponding to the existence of a two-phase reaction. For $CoSn_2$, the possible reaction leading to the formation of a Li_xCoSn_2 phase happens up to 1 Li. The second part of the electrochemical process occurs at very low voltage, i.e. between 0.14 and 0.0 V, during almost all the discharge process and can thus be seen as a two-phase process plateau.

Ex situ ^{119}Sn Mössbauer spectra of pristine materials and electrodes at the end of the first discharge are shown in Fig. 4 and the values of the hyperfine parameters are given in Table 1.

For the Ni_3Sn_4 sample, there are two absorption peaks (Fig. 4a). The Ni_3Sn_4 structure contains two independent crystallographic Sn sites (4i, 4i); both fully occupied [13]. Therefore, the spectrum has been fit to two doublets with equal relative intensity. The ^{119}Sn Mössbauer spectrum of the pristine $CoSn_2$ is characterized by a doublet (Fig. 4c). There is only one crystallographic site (8h) for the Sn atoms in $CoSn_2$ [14]. ^{119}Sn Mössbauer spectroscopy measurements show, for the Ni_3Sn_4 (Fig. 4b) and $CoSn_2$ (Fig. 4c) electrodes at the end of the first discharge, the appearance of two more contributions. The hyperfine parameters of these additional contributions are close to those found for the mechanically ball-milled synthesized Li_7Sn_2 alloy [15]. The formation of a Li_7Sn_2 nano-alloy as the final electrochemical lithiated product has already been reported with Cu_6Sn_5 [16], Cu_6Sn_5 with NiAs-type structure, space group $P6_3/mmc$ [17]. This shows that the structure of the pristine tin-based intermetallic material has no influence on the composition of the final electrochemical lithiated product.

Table 1
Hyperfine parameters obtained from the ^{119}Sn Mössbauer spectra shown in Fig. 4: the different types of tin sites used in the Mössbauer fitting procedure and their relative intensity I, the values of the isomer shift δ, the quadrupole splitting Δ and the line width at half maximum 2Γ

Sample	Alloys	Tin sites	I (%)	δ (mm/s)	Δ (mm/s)	2Γ (mm/s)
(a)	Ni_3Sn_4	4i	50	2.01 (4)	0.70 (6)	1.02 (4)
		4i	50	2.02 (4)	1.18 (6)	1.02 (3)
(b)	Ni_3Sn_4	4i	12	1.95 (12)	0.63 (27)	0.95 (3)
		4i	12	1.98 (6)	1.37 (10)	0.95 (3)
	Li_7Sn_2	4i	38	1.88 (5)	0.29 (11)	0.91 (3)
		4h	38	2.00 (6)	0.97 (9)	0.91 (3)
(c)	$CoSn_2$	8h	100	2.14 (3)	0.77 (3)	0.98 (4)
(d)	$CoSn_2$	8h	20	2.14 (3)	0.77 (3)	1.02 (3)
	Li_7Sn_2	4i	40	1.86 (4)	0.24 (3)	0.94 (7)
		4h	40	1.95 (4)	0.94 (6)	0.94 (7)

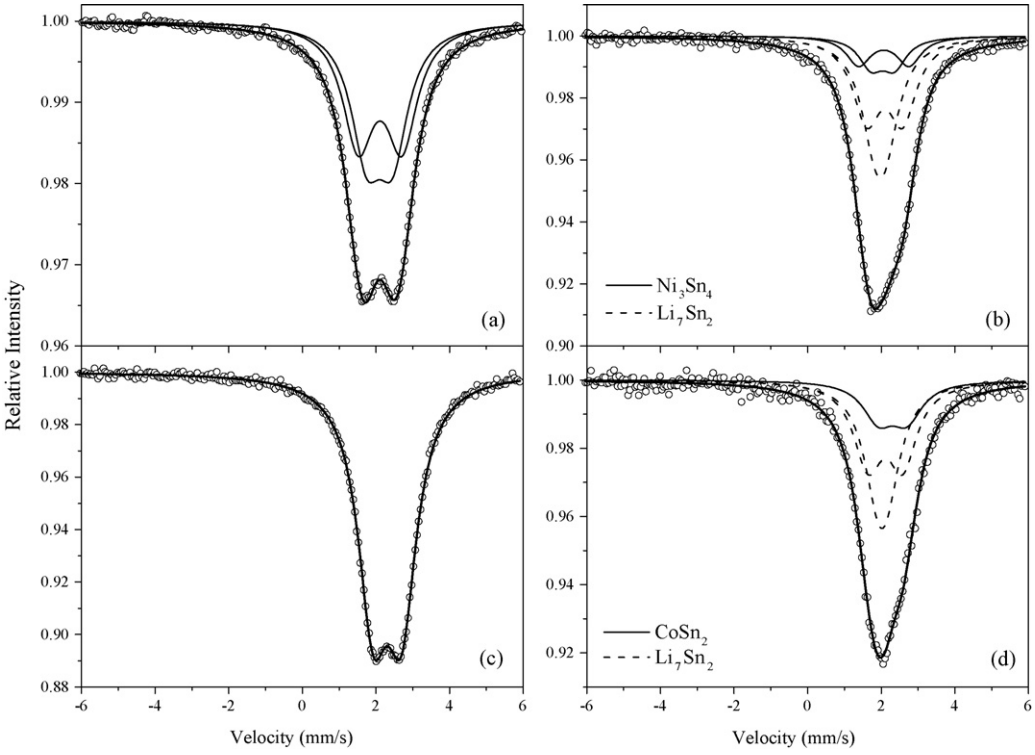

Fig. 4. *Ex situ* ^{119}Sn Mössbauer spectrum of (a) the pristine Ni_3Sn_4, (b) the Ni_3Sn_4 electrode at the end of the first discharge, (c) the pristine $CoSn_2$ and (d) the $CoSn_2$ electrode at the end of the first discharge.

However, the substitution/extraction reactions occurring on the plateaus are not complete and the contribution of the unreacted Ni_3Sn_4 and $CoSn_2$ are 24% and 20%, respectively. This may be due to the particle size and can explain the irreversibility and capacity fading during cycling.

4. Conclusion

Two tin-based intermetallic compounds, Ni_3Sn_4 and $CoSn_2$ have been investigated as anode materials. Various two-step alloying reactions have been observed with these intermetallic electrodes, i.e. the formation of a SEI and a possible solid-solution insertion reaction followed by a substitution/extraction reaction to directly form Li_7Sn_2. This shows that, no matter the crystal structure of the pristine materials, the Li-rich Li_7Sn_2 alloy is formed at the end of the first discharge. In these conditions, the reaction of these compounds to lithium is not complete. This may be explained by the fact that: (i) the particles of the bulk materials are oversized or (ii) the electrode manufacturing and cycling rate are not appropriate. At present, additional work is in progress in order to optimize the powder morphology.

Acknowledgements

This work has been carried out in the framework of ALISTORE, network of Excellence (contract No. SES6-CT-2003-503532). The authors are grateful to the European Community for financial support. C.M. Ionica-Bousquet acknowledges ADEME, France and SAFT Bordeaux, France (contract No. 752295/00) for financial support.

References

[1] J. Yang, Y. Takeda, N. Imanishi, J.Y. Xie, O. Yamamoto, J. Power Sources 97–98 (2001) 216–218.
[2] I.A. Courtney, W.R. McKinnon, J.R. Dahn, J. Electrochem. Soc. 146 (1999) 59–68.
[3] F. Robert, F. Morato, J. Chouvin, L. Aldon, P.-E. Lippens, J. Olivier-Fourcade, J.-C. Jumas, B. Simon, P. Biensan, J. Power Sources 119–121 (2003) 581–584.
[4] L.Y. Beaulieu, D. Larcher, R.A. Dunlap, J.R. Dahn, J. Electrochem. Soc. 147 (2000) 3206–3212.
[5] O. Mao, R.A. Dunlap, J.R. Dahn, J. Electrochem. Soc. 146 (1999) 405–413.
[6] I. Amadei, S. Panero, B. Scrosati, G. Cocco, L. Schiffini, J. Power Sources 143 (2005) 227–230.
[7] S. Sharma, L. Fransson, E. Sjöstedt, L. Nordström, B. Johansson, K. Edström, J. Electrochem. Soc. 150 (2003) A330–A334.
[8] H. Tanizaki, A. Omaru, US Patent 0,053,131 A1 (2004), to Sony Corporation.
[9] R.W. Cheary, A.A. Coelho, J. Appl. Cryst. 25 (1992) 109–121.
[10] K. Ruebenbauer, T. Birshall, Hyperfine Interact. 7 (1979) 125–133.
[11] V. Eshkenazi, E. Peled, L. Burstein, D. Golodnitsky, Solid State Ionics 170 (2004) 83–91.
[12] S. Naille, P.-E. Lippens, F. Morato, J. Olivier-Fourcade, Hyperfine Interact. 167 (2006) 785–790.
[13] W. Jeitschko, B. Jaberg, Acta Cryst. B 38 (1982) 598–600.
[14] E.E. Havinga, H. Damsma, P. Hokkeling, J. Less-Common Met. 27 (1972) 169–186.
[15] F. Robert, P.-E. Lippens, J. Olivier-Fourcade, J.-C. Jumas, F. Gillot, M. Morcrette, J.-M. Tarascon, J. Solid State Chem. 180 (2007) 413–422.
[16] W. Choi, J.Y. Lee, H.S. Lim, Electrochem. Commun. 6 (2004) 816–820.
[17] A. Gangulee, G.C. Das, M.B. Bever, Metall. Trans. 4 (1973) 2063–2066.